Spin current transport in hybrid Pt / multifunctional magnetoelectric Ga0.6Fe1.4O3 bilayers

Suvidyakumar Homkar, Elodie Martin, Benjamin Meunier, Alberto Anadon-Barcelona, Corinne Bouillet, Jon Gorchon, Karine Dumesnil, Christophe Lefèvre, François Roulland, Olivier Copie, et al.

Spin current transport in hybrid Pt / multifunctional magnetoelectric $Ga_{0.6}Fe_{1.4}O_3$ bilayers

Suvidyakumar Homkar,[†] Elodie Martin,[‡] Benjamin Meunier,[†] Alberto Anadon-Barcelona,[‡] Corinne Bouillet,[†] Jon Gorchon,[‡] Karine Dumesnil,[‡] Christophe Lefèvre,[†] François Roulland,[†] Olivier Copie,[‡] Daniele Preziosi,[†] Sébastien Petit-Watelot,[‡] Juan-Carlos Rojas-Sánchez,*[,‡] and Nathalie Viart*[,†]

[†]*Université de Strasbourg, CNRS, IPCMS, UMR 7504, F-67000 Strasbourg, France*
[‡]*Université de Lorraine, CNRS, IJL, F-54000 Nancy, France*

ABSTRACT

The low power manipulation of magnetization is currently a highly sought-after objective in spintronics. Non ferromagnetic large spin-orbit coupling heavy metal (NM) / ferromagnet (FM) heterostructures offer interesting elements of response to this issue, by granting the manipulation of the FM magnetization by the NM spin Hall effect (SHE) generated spin current. Additional functionalities, such as the electric field control of the spin current generation, can be offered using multifunctional ferromagnets. We have studied the spin current transfer processes between Pt and the multifunctional magnetoelectric $Ga_{0.6}Fe_{1.4}O_3$ (GFO). In particular, *via* angular dependent magnetotransport measurements, we were able to differentiate between magnetic proximity effect (MPE)-induced anisotropic magnetoresistance (AMR) and spin Hall magnetoresistance (SMR). Our analysis shows that SMR is the dominant phenomenon at all temperatures and is the only one to be considered near room temperature, with a magnitude comparable to those observed in Pd/YIG or Pt/YIG heterostructures. These results indicate that magnetoelectric GFO thin films show promises for achieving an electric-field control of the spin current generation in NM/FM oxide-based heterostructures.

ABSTRACT GRAPHIC
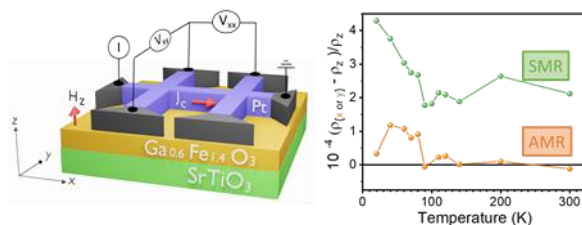
KEYWORDS: magnetic oxides thin films, gallium ferrite, platinum, spintronics, spin Hall magnetoresistance, magnetic proximity effects

1. INTRODUCTION

Non ferromagnetic heavy metal (NM) / ferromagnet (FM) heterostructures are currently largely investigated to study viable routes to exploit the fascinating interplay between heat, charge and spin transport.[1–3] In particular, recent developments point at a suitable low-power manipulation of magnetization in spintronic devices through spin-orbit torques (SOT) effects, which ground on the intrinsic spin-orbit coupling. Indeed, it has been shown that the spin current generated upon the application of a charge current in the heavy metal nonmagnetic material *via* the spin Hall effect (SHE) can manipulate the magnetic moments in the adjacent ferromagnetic (FM) layer through SOT.[4–10] This has triggered the development of a new Magnetic Random Access Memory (MRAM)-based technology, the spin-orbit torque MRAM (SOT-MRAM)[8], and the possibility to integrate SHE-based spin-valves in standard CMOS-like networks has already been demonstrated via complementary spintronic logic (CSL) design methodology.[11]

The interest for NM/FM heterostructures has recently moved from all-metal systems to systems in which the FM is an insulating oxide (FMI), and display the interesting phenomenon of spin Hall magnetoresistance (SMR).[12–14] The most emblematic NM/FMI system is based on garnet ferrite, with Pt/YIG ($Y_3Fe_5O_{12}$).[3,15–22] However, spinel ferrites have also been considered so far, with systems such as $Pt/NiFe_2O_4$,[3,18] Pt/Fe_3O_4[18] and $Pt/CoFe_2O_4$.[23–25] Recently, a study on $Pt/Bi_{0.9}La_{0.1}FeO_3$ bilayers[26] made a step towards the exciting challenge of the electric field control of the spin Hall effect. This, by granting the control of the generation of spin current in engineered NM/FM-based devices, adds extra functionalities to the realization of future spintronics devices.

Here we propose the use of another oxide, the multifunctional magnetoelectric gallium ferrite $Ga_{2-x}Fe_xO_3$ (GFOx, $0.8 \le x \le 1.4$),[27,28,29] with a view to use its magnetoelectric character in the future for an electric field control of the spin current generation from NM/FM heterostructures. $Ga_{2-x}Fe_xO_3$ crystallizes in the polar orthorhombic $Pna2_1$ (equivalently $Pc2_1n$) space group (S.G.#33),[30,31] different from the usual perovskite structure adopted by most of the other magnetoelectric compounds, with a = 0.5086(2) nm, b = 0.8765(2) nm, and c = 0.9422(2) nm for x = 1.4.[32] The material is polar with a polarization of ca. 25 $\mu C/cm^2$,[33,34] and ferrimagnetic with a Curie temperature increasing with x and reaching values above room temperature for x=1.3.[28,35,36] Taking into consideration the lattice matching possibilities, thin

films of GFOx (00*l*) can be epitaxially deposited on various substrates such as yttrium stabilized zirconia (001) (YSZ),[37,38] YSZ (111),[38] Pt (111) buffered YSZ (111)[37] or strontium titanate $SrTiO_3$ (111) (STO).[38,39] For symmetry reasons, while the (100) YSZ substrates allow the growth of six in-plane variants, the YSZ (111), Pt (111) buffered YSZ (111) and STO (111) ones will only allow three, the lowest number observed until now. GFO1.4 films were shown to be ferroelectric at room temperature,[39] to have a magnetic Curie temperature of ca. 370 K, and a saturation magnetization of about 100 emu/cm^3 at room temperature.[37,40]

2. MATERIALS ELABORATION AND CHARACTERIZATION - EXPERIMENTAL DETAILS

Here we show results obtained from Pt/GFO1.4 heterostructures which, for convenience, will be simply indicated as Pt/GFO. These heterostructures were deposited onto $SrTiO_3$ (111) (STO) substrates (Furuuchi Chemical Corporation, Japan, with rms-roughness lower than 0.15 nm), by pulsed laser deposition using a KrF excimer laser (λ= 248 nm) with a fluence of 4 J/cm². The choice of STO as the substrate was dictated by the will to have the lowest number of in-plane variants, and we have recently demonstrated the possibility to have a layer-by-layer growth of highly crystalline GFO on this substrate.[40] The growth of such atomically flat GFO films is a prerequisite to high quality Pt/GFO interfaces. The GFO layer (ca. 30 nm thick) was deposited first, at 900°C, by ablating a sintered stoichiometric $Ga_{0.6}Fe_{1.4}O_3$ ceramic target at a repetition rate of 2 Hz of in a 0.1 mbar O_2 pressure, using an already optimized procedure described elsewhere.[40] The overall composition of the film has been assessed by energy dispersive X-ray spectroscopy (EDX) coupled to a scanning electron microscopy technique (JEOL 6700 F). The analysis was performed at 5 keV, ensuring a large surface sensitivity of the EDX signal. The Pt deposition was performed at a repetition rate of 10 Hz, under the system base pressure of $2 .10^{-8}$ mbar, and at room temperature to avoid any interdiffusion between the metal and oxide layers. The Pt thickness chosen here for generating spin currents was of 5 nm. This thickness has been evidenced by other works as optimum for SHE-induced spin currents from its associated spin diffusion length (λ_{sd}), spin memory loss (SML) at the interface[41] and spin Hall torque efficiency per applied electric field unit.[42] The surface of the STO//GFO/Pt heterostructure, observed by atomic force microscopy (AFM) with a Bruker ICON microscope operated in tapping mode, has a low rms roughness of 0.3 nm (Figure 1a). The roughness of a GFO layer of similar thickness (32 nm) deposited alone on a STO (111) substrate, without any

Pt layer on top, had already been previously characterized, and is also of about 0.3 nm.[40] Observations of the heterostructure cross section by transmission electron microscope (TEM) (JEOL 2100 F) allowed confirming the low roughness of the Pt/GFO interface. A composition profile was measured across the interface by energy dispersive X-ray spectroscopy (EDS) and showed that interdiffusion is limited in this system and restricted to a less than 2 nm wide zone (Figure 1b). X-ray diffraction was performed on the heterostructure with a Rigaku Smart Lab diffractometer equipped with a rotating anode (9 kW) and a monochromated copper radiation (1.54056 Å). Both GFO oxide and Pt metal layers of the heterostructure are well crystallised (Figure 1c). GFO is oriented along its [001] direction and Pt, along its [111] direction, on the STO (111). A layer-by-layer growth together with a smooth Pt/GFO interface are demonstrated by clear Laue oscillations for both GFO and Pt around their 004 and 111 reflections, respectively. Reflectivity measurements allowed us to determine that the precise thicknesses of the GFO and Pt layers are 36 and 5 nm, respectively. The magnetic properties of the heterostructure were studied with a superconducting quantum interference device vibrating sample magnetometer (SQUID VSM MPMS 3, Quantum Design). Temperature dependent measurements of the magnetization performed in field cooled and zero field cooled modes (not shown here) indicate a Curie temperature of 364 K. The sample indeed still shows a ferromagnetic behaviour at room temperature with a saturation magnetization of 100 emu/cm^3, as expected for this Fe/Ga ratio.[37] A highly anisotropic behaviour is evidenced from the in-plane and out-of-plane magnetization loops measurements (Figure 1d). The magnetization lies preferentially in-plane, in perfect agreement with the fact that the [100] and [001] crystallographic axes are, respectively, the easy and hard magnetic directions for GFO,[28] and are observed from X-ray characterizations to lie, respectively, in- and out-of-plane.
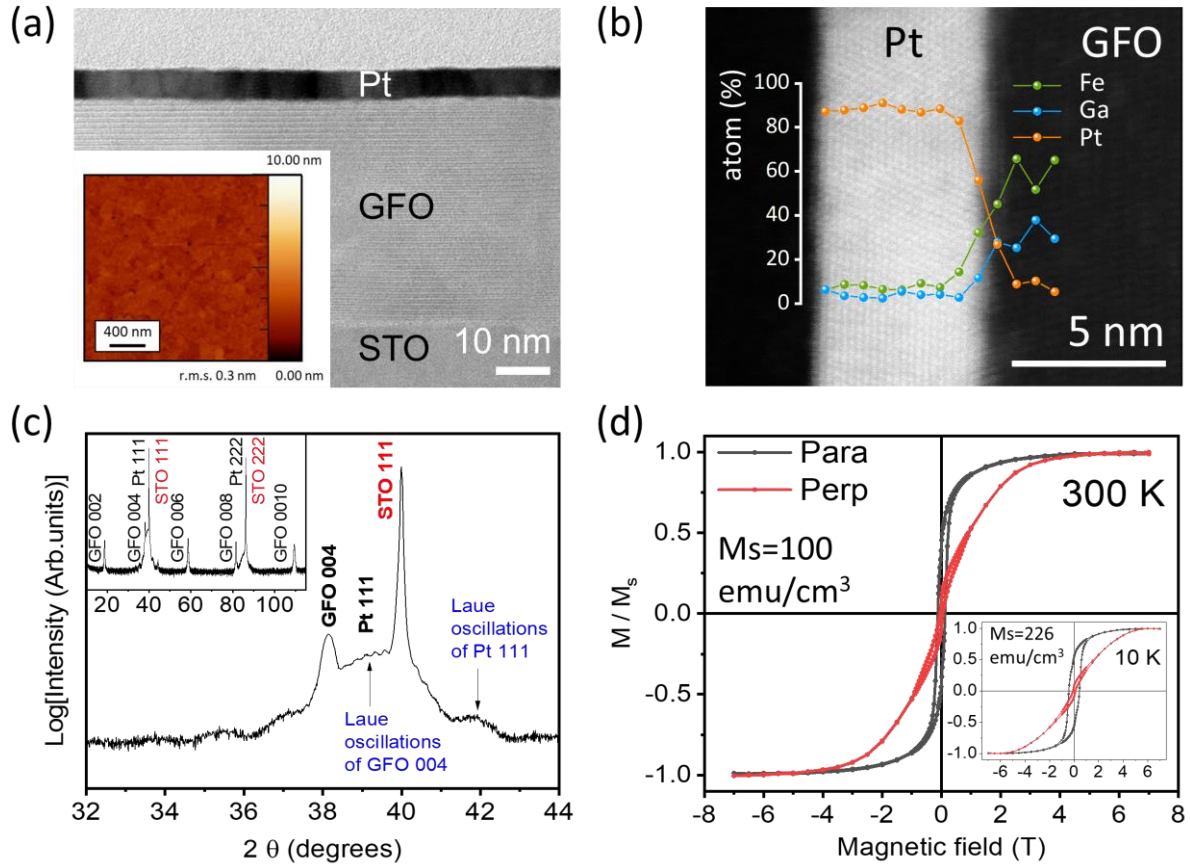
Figure 1. (a) TEM cross view of the STO//GFO(36 nm)/Pt(5 nm) heterostructure with (insert) the AFM image of its top surface indicating a rms roughness of 0.3 nm, (b) EDX mapping at the Pt/GFO interface, (c) X-ray diffractogram of the heterostructure in the θ-2θ mode, with a focus on the GFO 004 peak showing the Laue oscillations observed for both the GFO 004 and Pt layers 111 reflections, (d) Magnetization hysteresis loops of the heterostructure measured in both parallel and perpendicular modes at 300 K and (insert) 10 K.

3. MAGNETOTRANSPORT STUDY – RESULTS AND DISCUSSION

The Pt layer was patterned, using standard optical lithography, into double Hall bars to minimize the electrical resistance associated to the metallic contacts, with a longitudinal length L=38 µm, a width w=10 µm, and a thickness t=5 nm (Figure 2). The current is injected in the Pt bar along the STO[0-11] (ΓM) direction, that is, perpendicularly to the [100] easy magnetization direction of GFO. The plane of the films will be referred to as xy, and the normal to the film will be named z. H_z (H_x, H_y) refers to the magnetic field applied along the z (x, y) direction. The electric current density J_c is applied along x, and the longitudinal (transversal) resistivity ρ_{xx} (ρ_{xy}) is calculated from the measured voltage V_{xx} (V_{xy}).
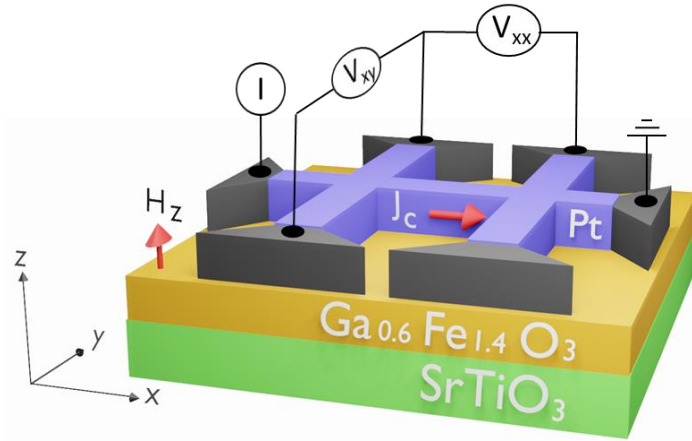
Figure 2. Schematics of the lithographed double Hall bars on STO//GFO(36 nm)/Pt(5 nm) heterostructures with indications of length (L), width (w) and thickness (t).

Magnetotransport in heavy metal (NM) / insulating ferromagnet (FMI) heterostructures may involve contributions from two main origins: (1) the magnetic proximity effect (MPE), and (2) the spin Hall related effects with the spin Hall magnetoresistance (SMR). Figure 3 offers a schematic representation of the microscopic mechanisms behind each contribution and for two different geometries of measurement, *i.e.* longitudinal and transverse.

Going to details, MPE implies the existence of some induced interfacial magnetism in the non-magnetic Pt layer. As a result, anisotropic magnetoresistance (AMR) and anomalous Hall effects[43] (AHE), characteristic of metallic FM, can play a role.

Instead, SMR contribution does not necessitate the existence of any MPE as already put forward by Nakayama *et al.*[14] SMR effects arise as a combination of the spin Hall effect (SHE) and the inverse spin Hall effect (ISHE). When a charge current flows longitudinally in the nonmagnetic NM, a spin current is produced along the film normal direction by SHE. The spin polarization $\vec{\sigma}$ of this spin current is perpendicular to both charge and spin current densities, $\vec{J_e}$ and $\vec{J_s}$, respectively, in agreement with $\vec{J_s} = \theta_{SH}(\vec{\sigma} \times \vec{J_e})$, where θ_{SH} is the spin Hall angle.[44,45] The spin current can either be reflected or absorbed by the adjacent FM layer depending on whether $\vec{\sigma}$ is parallel or perpendicular to the magnetization direction of the FM layer, respectively.[18] The reflected spin current will produce an additional charge current through the inverse spin Hall effect (ISHE) which will lead to a decrease of the longitudinal resistivity. The resistivity of the NM layer will therefore strongly depend upon the orientation of the FM magnetization.

If one neglects contributions from other phenomena such as the topological Hall effect[46] (THE) or unidirectional magnetoresistance[47,48] (UMR), very unlikely in this collinear-spins system, the longitudinal (ρ_{xx}) and transverse (ρ_{xy}) resistivities of the studied heterostructure as a function of an external magnetic field can be described by the following equations:[13,18]

$$\rho_{xx} = \rho_0 + \Delta\rho_{MPE\ AMR} \cdot m_x^2 + \Delta\rho_{||SMR} \cdot m_y^2 \tag{1}$$

$$\rho_{xy} = (\Delta\rho_{MPE\ PHE} - \Delta\rho_{||SMR}) \cdot m_x \cdot m_y + (\Delta\rho_{MPE\ AHE} + \Delta\rho_{\perp\ SMR}) \cdot m_z \tag{2}$$

where m_x, m_y, and m_z are the magnetization unit vector components in the x, y, and z directions, respectively, ρ_0 is the resistivity of platinum in the absence of a magnetic field, $\Delta\rho_{MPE\ AMR}$ is the anisotropic magneto-resistivity due to the MPE induced anisotropic magnetoresistance (MPE AMR), and $\Delta\rho_{MPE\ PHE\ (AHE)}$ is the planar (anomalous) Hall resistivity due to the MPE induced planar (anomalous) Hall effect in the NM. The AMR and AHE contributions, which depend on the orientation of the MPE-induced magnetic Pt, arise due to extrinsic spin-flip scattering mechanism and/or intrinsic mechanism depending on the band structure of Pt. In addition, one has to consider the SMR related phenomena. $\Delta\rho_{||SMR}$ represents the SMR effect and $\Delta\rho_{\perp\ SMR}$ is a Hall-effect-type resistivity that can be relevant in systems where the imaginary part of the spin mixing conductance is important, but it is usually smaller than $\Delta\rho_{||SMR}$.[18]

Magnetic Proximity Effect (MPE)　　　　**Spin Hall Effects (SHE)**

$$\rho_{xx} = \rho_0 + \Delta\rho_{MPE\ AMR} \cdot m_x^2$$

$$\rho_{xx} = \rho_0 + \Delta\rho_{||\ SMR} \cdot m_y^2$$

(a) AMR

(b) Longitudinal SMR

$$\rho_{xy} = \Delta\rho_{MPE\ PHE} \cdot m_x \cdot m_y + \Delta\rho_{MPE\ AHE} \cdot m_z$$

$$\rho_{xy} = -\Delta\rho_{||\ SMR} \cdot m_x \cdot m_y + \Delta\rho_{\perp\ SMR} \cdot m_z$$

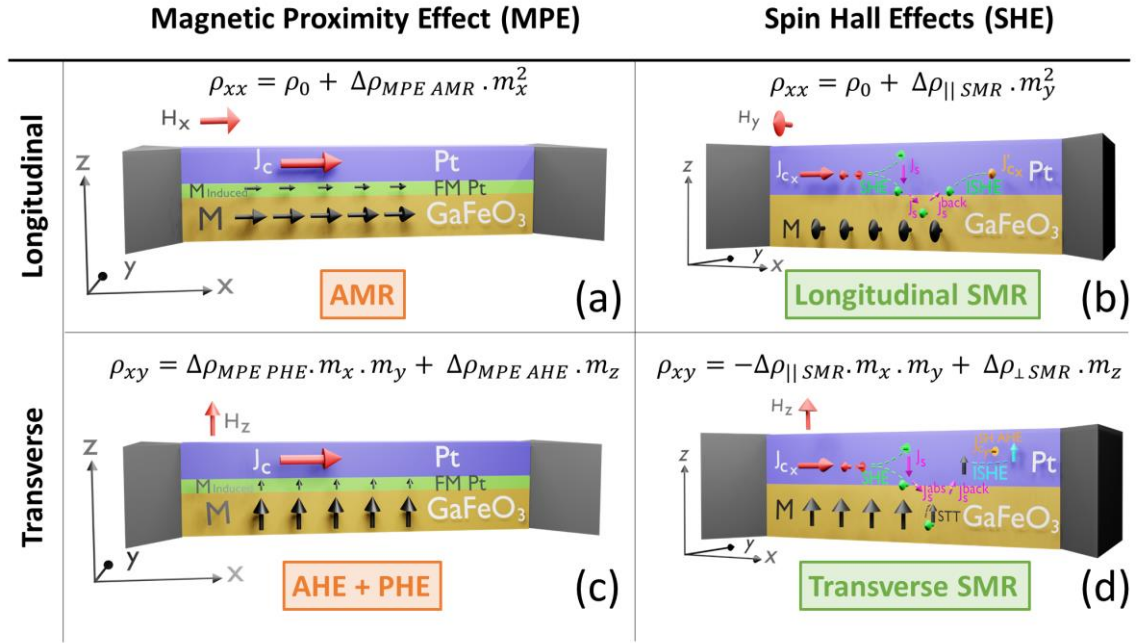(c) AHE + PHE

(d) Transverse SMR

Figure 3. Schematics of the various physical phenomena which have to be considered for magnetotransport in a Pt/GFO heterostructure, for both longitudinal, (a) and (b), and transverse, (c) and (d), modes involving the magnetic proximity effects (MPE) with anisotropic magnetoresistance (AMR), anomalous Hall effect (AHE) and planar Hall effect (PHE), and the spin Hall induced effects (SHE).

Longitudinal magnetoresistance

The longitudinal magnetoresistance (MR) is defined as $\frac{\rho_{xx\ (H)} - \rho_{xx\ (H=7T)}}{\rho_{xx\ (H=7T)}} = \frac{\Delta\rho_{xx}}{\rho_{xx}}(H)$. The field dependence of the MR (for a field applied along the z direction) is plotted in Figure 4a for various temperatures between 20 and 300 K. These curves are a clear evidence of the presence of non-zero longitudinal magnetoresistance (MR). The MR decreases with increasing temperature, goes to zero at approximately 120 K, after what it keeps a negligible value (Figure 4b). This behavior of MR cannot be attributed to weak localization (WL) and weak anti-localization (WAL) mechanisms. If one cannot completely exclude the existence of a 2DEG at the STO/GFO interface, it will however not be possible to observe any of its transport properties in the Pt layer, where the electrical contacts are made, because of the insulating character of the GFO layer between the STO and Pt layers. Moreover, the temperatures at which WL and WAL are at play are usually much lower than 120 K, since such quantum effects require that the coherence of the wave functions is kept. Possible origins behind the temperature evolution of the MR will be discussed later. The MR curves presented in Figure 4a do not saturate even at magnetic fields beyond the magnetic saturation of the

heterostructure observed by SQUID (Figure 1d). This is probably caused by some independent moments at the interface.[49] It can be related to the highly anisotropic nature of magnetism in the GFO films, which induces high anisotropy for the induced magnetic Pt as well, through a magnetic proximity effect, and will inhibit a saturation point even at high temperatures. The measured Pt resistivity value of 23 $\mu\Omega$.cm at room temperature is in good agreement with values reported for Pt thin films deposited either by sputtering or molecular beam epitaxy.[50,51] Its linear decrease with temperature is also in agreement with previous studies.[52]
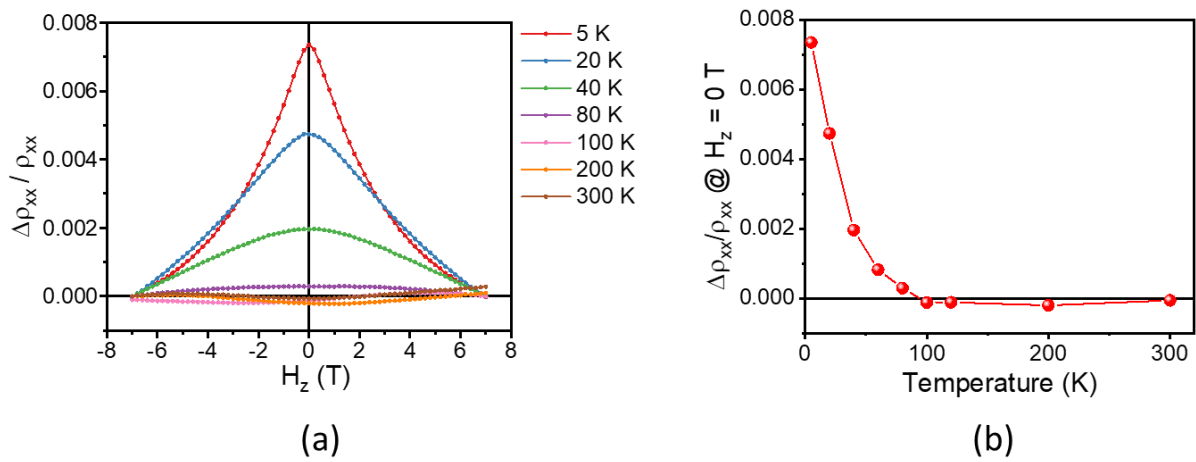

Figure 4. Longitudinal magnetoresistance (as defined in the main text). (a) Measurements at various temperatures, and (b) Temperature dependence of the longitudinal magnetoresistance estimated for H_z= 0 T.

Transverse magnetoresistance

The magnetic field dependence of the transverse Hall resistivity ρ_{xy} measured at various temperatures between 20 and 300 K (the field is applied along the z direction), is presented in Figure 5a, after correction from both the ordinary magneto-resistance (OMR) contribution due to the variation of the temperature and the ordinary Hall resistance (OHR) due to the Lorentz force applied onto the carriers. For all temperatures, this corrected transverse resistivity $\rho_{xy-corr}$ behaves as an odd function (opposed signs for opposed Hz fields). In the light of Equation (2), this means that it results from the contribution of the second term, $(\Delta\rho_{MPE\ AHE} + \Delta\rho_{\perp\ SMR})$. The first one, associated to in-plane projections of magnetization, is not expected to reverse with reversing Hz fields.

One can observe a sign reversal of the $\rho_{xy-corr}$ signal with temperature on Figure 5a. A more precise estimation of the temperature at which this sign reversal operates can be done by plotting the temperature dependence of the values measured for $\rho_{xy-corr}$ at 7 T (Figure 5b). The inversion temperature is of about 120 K, which is the same as the one at which the longitudinal resistivity ρ_{xx} goes to zero (Figure 4b). A sign inversion of the transverse resistivity has already been observed for Pt/YIG systems and assigned to AHE-induced by MPE in the Pt.[15,19,53] Similar temperature variations of the AHE were also observed in the absence of any FM layer, in ion-gated platinum thin films and analogously attributed to some induced ferromagnetic ordering on the Pt surface.[16,54] The explanation given by Zhou *et al.*[53] for such a sign inversion is that for paramagnetic Pt, both the density of states (DOS) and curvature near the Fermi surface importantly change with temperature. They indeed observed, for Pt/YIG heterostructures, a sign inversion of the ordinary Hall coefficient R_0 of Pt with temperature, indicating a change of the carriers type. The raw resistivity curves we measured, before OMR and OHR corrections, are shown in SI, Figure S1. The ordinary Hall coefficient of Pt, R_0, determined as the slope of the linear part of the measurements at high magnetic fields, is always negative and does not vary significantly with temperature. It allows determining a free electron density in Pt of $48 . 10^{28}$ /m^3 , in good agreement with values expected for a metal[55] and already reported for other Pt thin films.[15,16] The absence of any sign inversion of R_0 in our case could originate from the fact that we have used a thicker Pt layer (5 nm) than the one used by Zhou *et al.* (1 nm).[53] Shimizu *et al.*,[16] who have used 3.5 nm thick Pt layers, also observe a constant negative R_0. The modification of the DOS and curvature near the Fermi surface, induced by a MPE, is indeed expected to happen only at the interface between the NM and FM materials, and could be masked in our case, for which the bulk signature predominates. We cannot therefore be fully conclusive on the incidence of MPE-induced AHE on the temperature behaviour of transverse resistivity.

In order to go further in the understanding of our system, we have sought to disentangle the MPE-based and SMR contributions in the longitudinal measurements.
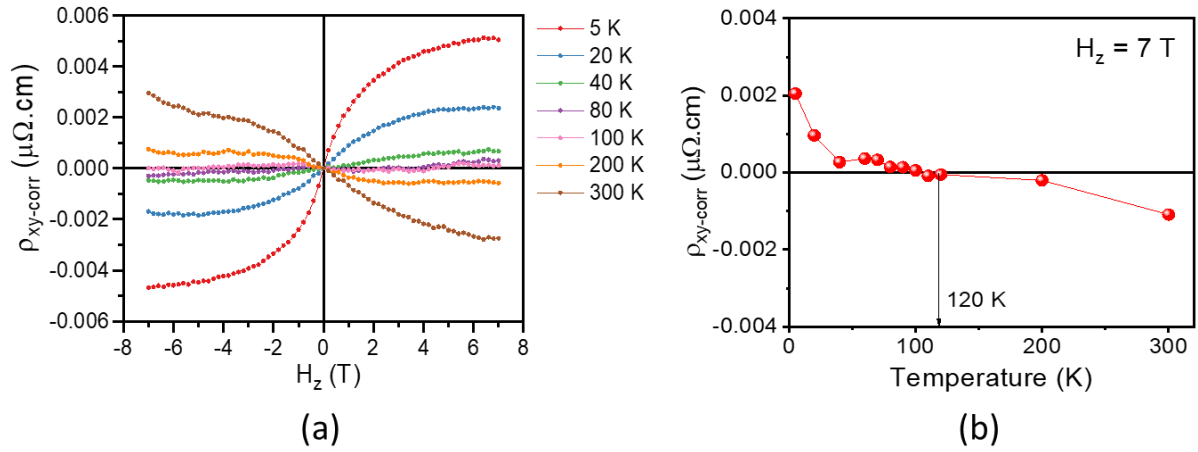
Figure 5. Transverse Hall resistivity measurements with (a) Transverse resistivity corrected from both the ordinary magnetoresistance and the linear contribution of the ordinary Hall effect (for a selection of temperatures), (b) Temperature dependence of the transverse resistivity at H_z = 7 T.

Angular dependence of the longitudinal resistivity

One possible way to distinguish between the MPE-based AMR and SMR contributions is through the insertion of a nonmagnetic metal such as Cu or of an antiferromagnetic oxide such as NiO, which might eliminate the possibility of MPE effects, leaving only SMR effects to play a role. However, this introduces additional interfacial issues and important modifications of the SMR, depending upon the interlayer thickness, have been reported in both Pt/Cu/Co/Pt[56] and Pt/NiO/YIG[57] heterostructures.

An alternative way to separate AMR and SMR contributions is by performing angle-dependent longitudinal measurements with the magnetic field in either the xz or the yz planes, while the current density J_c and the measured resistivity ρ_{xx} are in the x direction[49] as schematized in Figure 6a. This can be understood from Equation 1: a rotation of the magnetic field within the yz (xz) plane will only have an effect on the SMR (AMR) and no effect on the AMR (SMR) which only depends on M_x (M_y). As depicted in Figure 3, while the AMR results from the fact that M is parallel to the current direction, the SMR originates from the fact that M is parallel to the spins of the electrons of the SHE-generated spin current, which prevents the spins to be absorbed by the FM, and causes them to be reflected into Pt.[14]

We measured ρ_{xx} at H = 7 T while rotating the sample in the yz (xz) plane to study the β (α) angle dependence of ρ_{xx}, at various temperatures. The orientation of the magnetic field is described through the α (within the xz plane) and β (within the yz plane) angles. For the

experiments, the α and β angles were limited to a 90° rotation, and conventionally, the z direction was chosen as the 90° angle. Both $\frac{\rho(\beta)-\rho_z}{\rho_z}$, and $\frac{\rho(\alpha)-\rho_z}{\rho_z}$ calculated quantities are shown in Figure 6b for various temperatures. The β-dependent measurements show that the resistivity value decreases when going from H_z to H_y at all temperatures, with a 180° periodic oscillation. On the other side, the α measurements also show that the resistivity value decreases when going from H_z to H_x but with a smaller change in resistivity, and no unambiguous periodic oscillation. By fitting the β measurements with $\cos^2\beta$ (SI, Figure S2), the $\frac{\rho_y-\rho_z}{\rho_z}$ SMR values can be extracted. The α measurements could not unambiguously be fitted with $\cos^2\alpha$, and the $\frac{\rho_x-\rho_z}{\rho_z}$ MPE AMR values are extracted from the $\frac{\rho(\alpha)-\rho_z}{\rho_z}$ measurements at α = 0°. This procedure is comforted by the fact that the values of $\frac{\rho_y-\rho_z}{\rho_z}$ (SMR), extracted from the β measurements, have the same values as $\frac{\rho(\beta)-\rho_z}{\rho_z}$ for β = 0°. Hence, assuming that the α measurements are periodic as well, we extracted the $\frac{\rho_x-\rho_z}{\rho_z}$ (AMR) values from $\frac{\rho(\alpha)-\rho_z}{\rho_z}$ measurements at α = 0°.

The SMR and AMR values obtained as explained are plotted in Figure 6c. Both contributions globally decrease with increasing temperatures. SMR shows a minimum at about 120 K, which is also the temperature at which AMR goes to zero. For all temperatures, the SMR contribution dominates over the AMR one, and it is the only one present above 120 K. The predominance of the SMR mechanism over the entire temperature range has also been observed for Pt/YIG and Pd/YIG samples. The SMR value measured for the Pt/GFO heterostructures is about 2 .10^{-4} at 300 K and 4.5 .10^{-4} at 20 K. These values are similar to what is observed in Pd/YIG heterostructures, and only slightly smaller than the ones observed in Pt/YIG (4 .10^{-4} at 300 K and 6 .10^{-4} at 20 K).[49] If the AMR contribution we observe is very similar to the one reported in other works[19,49,58,59]: same positive sign, similar amplitude of ca. 10^{-4}, and a decrease with increasing temperature which leaves it practically insignificant after about 100 K, we however highlight some differences stemming from the temperature dependence of the SMR contribution. Studies performed under a high magnetic field, such as the present one of Pt/GFO performed at 7 T or the study of Pt/YIG under 100 kOe,[49] show V-shaped SMR curves, with first a decrease and then an increase with the increasing temperature, the position of the minimum varying between 20 and 120 K from one system to another. The measurements

performed in lower magnetic fields (10 kOe)[53,59] globally show an inversed tendency, with first an increase and then a decrease, with a maximum at about 100 K.
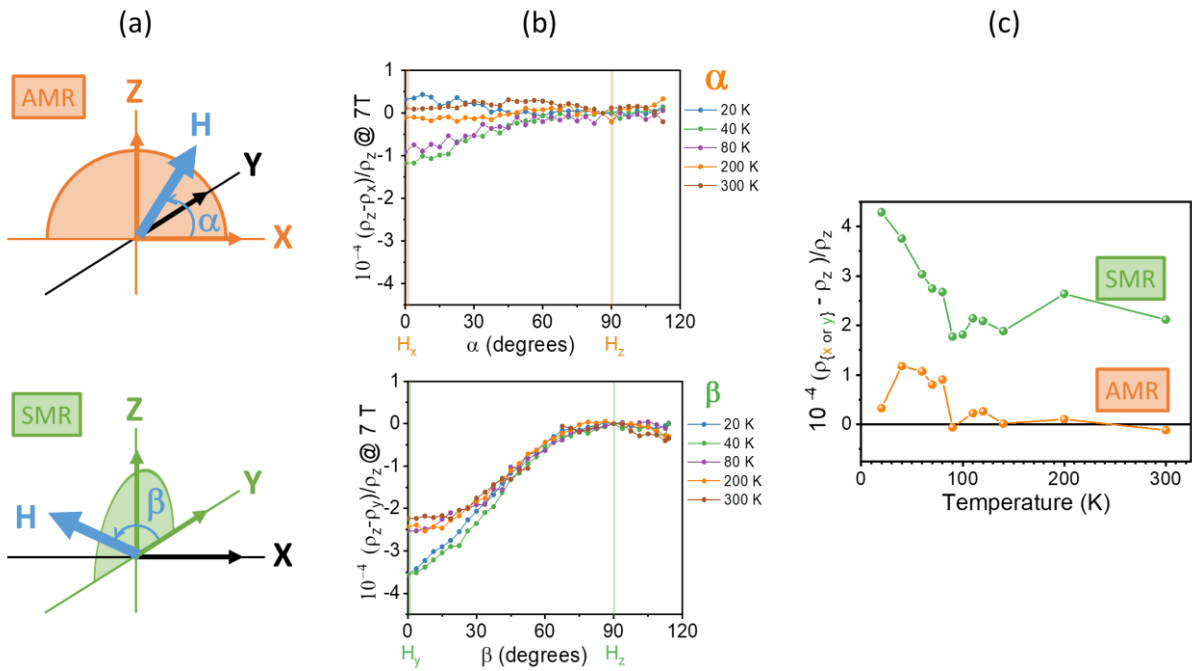

Figure 6. Identification of the SMR and AMR contributions to the longitudinal effects, (a) Geometries of the measurements, (b) Angular measurements at various temperatures (selection of temperatures) in both geometries, (c) Temperature dependence of SMR and AMR as deduced from the $\frac{\rho(\beta)-\rho_z}{\rho_z}$ and $\frac{\rho(\alpha)-\rho_z}{\rho_z}$ values measured at zero degree angle for β and α, respectively.

The magnetic state of the magnetic material is probably to be considered to explain such differences. Recently, a theoretical study has shown that the orbital hybridization of the magnetic material plays a role in the magnetoresistance, most probably in relation with spin-orbit coupling.[60] The minimum in SMR we observe here could thus be put in perspective with the modification of the spin-orbit coupling observed in bare GFO thin films near 120 K *via* our XMCD study.[61]

In fact, since both SMR and MPE-induced magnetoresistive contributions stem from the interaction between the charge current flowing in the Pt layer and the magnetic properties of the FM, the modification of the spin-orbit coupling at 120 K for GFO could contribute to the observed temperature variations of both longitudinal and transverse magnetoresistance measurements in the 90-140 K temperature range (Figures 4b and 5b).

4. CONCLUSION

The multifunctional magnetoelectric GFO oxide has successfully been introduced in FMI/NM (with Pt as the NM) heterostructures of high crystalline quality. The Pt/GFO interface is sharp and this makes the heterostructure suitable for spin currents transparency. The interactions between the spin Hall current from Pt and the GFO magnetic orientation have been evidenced by magnetotransport measurements. SMR has been shown to be the dominant phenomenon at all temperatures, and it is the only one to be considered near room temperature, with a magnitude comparable to those observed in the classically studied Pd/YIG or Pt/YIG heterostructures. This study therefore validates the use of GFO as a multifunctional magnetoelectric material in NM/FMI heterostructures with a view to control their spin current generation by an electric field.

SUPPORTING INFORMATION

Transverse Hall resistivity measurements, Fitting of the longitudinal angular dependent measurements

AUTHOR INFORMATION

Corresponding Authors

*E-mail: juan-carlos.rojas-sanchez@univ-lorraine.fr (J.-C.R.-S.)

*E-mail: viart@unistra.fr (N.V.)

REFERENCES

(1)   Slachter, A.; Bakker, F. L.; Adam, J.-P.; van Wees, B. J. Thermally Driven Spin Injection from a Ferromagnet into a Non-Magnetic Metal. *Nat. Phys.* **2010**, *6* (11), 879–882. https://doi.org/10.1038/nphys1767.

(2)   Ando, K.; Takahashi, S.; Ieda, J.; Kajiwara, Y.; Nakayama, H.; Yoshino, T.; Harii, K.; Fujikawa, Y.; Matsuo, M.; Maekawa, S.; Saitoh, E. Inverse Spin-Hall Effect Induced by Spin Pumping in Metallic System. *J. Appl. Phys.* **2011**, *109* (10), 103913. https://doi.org/10.1063/1.3587173.

(3)   Meier, D.; Reinhardt, D.; van Straaten, M.; Klewe, C.; Althammer, M.; Schreier, M.; Goennenwein, S. T. B.; Gupta, A.; Schmid, M.; Back, C. H.; Schmalhorst, J.-M.; Kuschel, T.; Reiss, G. Longitudinal Spin Seebeck Effect Contribution in Transverse Spin Seebeck Effect Experiments in Pt/YIG and Pt/NFO. *Nat. Commun.* **2015**, *6* (1), 8211. https://doi.org/10.1038/ncomms9211.

(4)   Kajiwara, Y.; Harii, K.; Takahashi, S.; Ohe, J.; Uchida, K.; Mizuguchi, M.; Umezawa, H.; Kawai, H.; Ando, K.; Takanashi, K.; Maekawa, S.; Saitoh, E. Transmission of Electrical Signals by Spin-Wave Interconversion in a Magnetic Insulator. *Nature* **2010**, *464* (7286), 262-U141. https://doi.org/10.1038/nature08876.

(5)   Liu, L.; Lee, O. J.; Gudmundsen, T. J.; Ralph, D. C.; Buhrman, R. A. Current-Induced Switching of Perpendicularly Magnetized Magnetic Layers Using Spin Torque from the Spin Hall Effect. *Phys. Rev. Lett.* **2012**, *109* (9), 096602–096602.

(6)   Liu, L.; Pai, C.-F.; Li, Y.; Tseng, H. W.; Ralph, D. C.; Buhrman, R. A. Spin-Torque Switching with the Giant Spin Hall Effect of Tantalum. *Science* **2012**, *336*, 555.

(7)   Manchon, A.; Železný, J.; Miron, I. M.; Jungwirth, T.; Sinova, J.; Thiaville, A.; Garello, K.; Gambardella, P. Current-Induced Spin-Orbit Torques in Ferromagnetic and Antiferromagnetic Systems. *Rev. Mod. Phys.* **2019**, *91* (3), 035004. https://doi.org/10.1103/RevModPhys.91.035004.

(8)   Mihai Miron, I.; Garello, K.; Gaudin, G.; Zermatten, P.-J.; Costache, M. V.; Auffret, S.; Bandiera, S.; Rodmacq, B.; Schuhl, A.; Gambardella, P. Perpendicular Switching of a Single Ferromagnetic Layer Induced by In-Plane Current Injection. *Nature* **2011**, *476* (7359), 189-U88. https://doi.org/10.1038/nature10309.

(9)   Rojas-Sánchez, J.-C.; Laczkowski, P.; Sampaio, J.; Collin, S.; Bouzehouane, K.; Reyren, N.; Jaffrès, H.; Mougin, A.; George, J.-M. Perpendicular Magnetization Reversal in Pt/[Co/Ni]₃/Al Multilayers via the Spin Hall Effect of Pt. *Appl. Phys. Lett.* **2016**, *108* (8), 082406.

(10)   Pham, T. H.; Je, S.-G.; Vallobra, P.; Fache, T.; Lacour, D.; Malinowski, G.; Cyrille, M. C.; Gaudin, G.; Boulle, O.; Hehn, M.; Rojas-Sánchez, J.-C.; Mangin, S. Thermal Contribution to the Spin-Orbit Torque in Metallic-Ferrimagnetic Systems. *Phys. Rev. Appl.* **2018**, *9* (6), 064032. https://doi.org/10.1103/PhysRevApplied.9.064032.

(11)   Kang, W.; Wang, Z.; Zhang, Y.; Klein, J.-O.; Lv, W.; Zhao, W. Spintronic Logic Design Methodology Based on Spin Hall Effect-Driven Magnetic Tunnel Junctions. *J. Phys. -Appl. Phys.* **2016**, *49* (6), 65008–65008.

(12)   Chen, Y.-T.; Takahashi, S.; Nakayama, H.; Althammer, M.; Goennenwein, S. T. B.; Saitoh, E.; Bauer, G. E. W. Theory of Spin Hall Magnetoresistance. *Phys. Rev. B* **2013**, *87* (14). https://doi.org/10.1103/PhysRevB.87.144411.

(13)   Chen, Y.-T.; Takahashi, S.; Nakayama, H.; Althammer, M.; Goennenwein, S. T. B.; Saitoh, E.; Bauer, G. E. W. Theory of Spin Hall Magnetoresistance (SMR) and Related Phenomena. *J. Phys. Condens. Matter* **2016**, *28* (10), 103004. https://doi.org/10.1088/0953-8984/28/10/103004.

(14)   Nakayama, H.; Althammer, M.; Chen, Y. T.; Uchida, K.; Kajiwara, Y.; Kikuchi, D.; Ohtani, T.; Gepraegs, S.; Opel, M.; Takahashi, S.; Gross, R.; Bauer, G. E. W.; Goennenwein, S. T. B.; Saitoh, E. Spin Hall Magnetoresistance Induced by a Nonequilibrium Proximity Effect. *Phys. Rev. Lett.* **2013**, *110* (20), 206601. https://doi.org/10.1103/PhysRevLett.110.206601.

(15)   Huang, S. Y.; Fan, X.; Qu, D.; Chen, Y. P.; Wang, W. G.; Wu, J.; Chen, T. Y.; Xiao, J. Q.; Chien, C. L. Transport Magnetic Proximity Effects in Platinum. *Phys. Rev. Lett.* **2012**, *109* (10), 107204. https://doi.org/10.1103/PhysRevLett.109.107204.

(16)   Shimizu, S.; Takahashi, K. S.; Hatano, T.; Kawasaki, M.; Tokura, Y.; Iwasa, Y. Electrically Tunable Anomalous Hall Effect in Pt Thin Films. *Phys. Rev. Lett.* **2013**, *111* (21), 216803. https://doi.org/10.1103/PhysRevLett.111.216803.

(17)   Vlietstra, N.; Shan, J.; Castel, V.; van Wees, B. J.; Ben Youssef, J. Spin-Hall Magnetoresistance in Platinum on Yttrium Iron Garnet: Dependence on Platinum Thickness and in-Plane/out-of-Plane Magnetization. *Phys. Rev. B* **2013**, *87* (18), 184421. https://doi.org/10.1103/PhysRevB.87.184421.

(18)   Althammer, M.; Meyer, S.; Nakayama, H.; Schreier, M.; Altmannshofer, S.; Weiler, M.; Huebl, H.; Geprägs, S.; Opel, M.; Gross, R.; Meier, D.; Klewe, C.; Kuschel, T.; Schmalhorst, J.-M.; Reiss, G.; Shen, L.; Gupta, A.; Chen, Y.-T.; Bauer, G. E. W.; Saitoh, E.; Goennenwein, S. T. B. Quantitative Study of the Spin Hall Magnetoresistance in Ferromagnetic Insulator/Normal Metal Hybrids. *Phys. Rev. B* **2013**, *87* (22), 224401. https://doi.org/10.1103/PhysRevB.87.224401.

(19)   Zhou, X.; Ma, L.; Shi, Z.; Fan, W. J.; Zheng, J.-G.; Evans, R. F. L.; Zhou, S. M. Magnetotransport in Metal/Insulating-Ferromagnet Heterostructures: Spin Hall Magnetoresistance or Magnetic Proximity Effect. *Phys. Rev. B* **2015**, *92* (6), 060402. https://doi.org/10.1103/PhysRevB.92.060402.

(20)   Evelt, M.; Safranski, C.; Aldosary, M.; Demidov, V. E.; Barsukov, I.; Nosov, A. P.; Rinkevich, A. B.; Sobotkiewich, K.; Li, X.; Shi, J.; Krivorotov, I. N.; Demokritov, S. O. Spin Hall-Induced Auto-Oscillations in Ultrathin YIG Grown on Pt. *Sci. Rep.* **2018**, *8* (1), 1269. https://doi.org/10.1038/s41598-018-19606-5.

(21)   Miao, B. F.; Huang, S. Y.; Qu, D.; Chien, C. L. Physical Origins of the New Magnetoresistance in Pt/YIG. *Phys. Rev. Lett.* **2014**, *112* (23), 236601. https://doi.org/10.1103/PhysRevLett.112.236601.

(22)   Vélez, S.; Golovach, V. N.; Bedoya-Pinto, A.; Isasa, M.; Sagasta, E.; Abadia, M.; Rogero, C.; Hueso, L. E.; Bergeret, F. S.; Casanova, F. Hanle Magnetoresistance in Thin Metal Films with Strong Spin-Orbit Coupling. *Phys. Rev. Lett.* **2016**, *116* (1), 016603. https://doi.org/10.1103/PhysRevLett.116.016603.

(23)   Amamou, W.; Pinchuk, I. V.; Trout, A. H.; Williams, R. E. A.; Antolin, N.; Goad, A.; O'Hara, D. J.; Ahmed, A. S.; Windl, W.; McComb, D. W.; Kawakami, R. K. Magnetic Proximity Effect in Pt/CoFe$_2$O$_4$ Bilayers. *Phys. Rev. Mater.* **2018**, *2* (1), 011401. https://doi.org/10.1103/PhysRevMaterials.2.011401.

(24)   Isasa, M.; Bedoya-Pinto, A.; Velez, S.; Golmar, F.; Sanchez, F.; Hueso, L. E.; Fontcuberta, J.; Casanova, F. Spin Hall Magnetoresistance at Pt/CoFe$_2$O$_4$ Interfaces and Texture Effects. *Appl. Phys. Lett.* **2014**, *105* (14), 142402. https://doi.org/10.1063/1.4897544.

(25) Vasili, H. B.; Gamino, M.; Gàzquez, J.; Sánchez, F.; Valvidares, M.; Gargiani, P.; Pellegrin, E.; Fontcuberta, J. Magnetoresistance in Hybrid $Pt/CoFe_2O_4$ Bilayers Controlled by Competing Spin Accumulation and Interfacial Chemical Reconstruction. *ACS Appl. Mater. Interfaces* **2018**, *10* (14), 12031–12041. https://doi.org/10.1021/acsami.8b00384.

(26) Gao, R.; Fu, C.; Cai, W.; Chen, G.; Deng, X.; Zhang, H.; Sun, J.; Shen, B. Electric Control of the Hall Effect in $Pt/Bi_{0.9}La_{0.1}FeO_3$ Bilayers. *Sci. Rep.* **2016**, *6* (1), 20330. https://doi.org/10.1038/srep20330.

(27) Roy, A.; Mukherjee, S.; Gupta, R.; Prasad, R.; Garg, A. Structure and Properties of Magnetoelectric Gallium Ferrite: A Brief Review. *Ferroelectrics* **2014**, *473* (1), 154–170. https://doi.org/10.1080/00150193.2014.923704.

(28) Arima, T.; Higashiyama, D.; Kaneko, Y.; He, J. P.; Goto, T.; Miyasaka, S.; Kimura, T.; Oikawa, K.; Kamiyama, T.; Kumai, R.; Tokura, Y. Structural and Magnetoelectric Properties of $Ga_{2-x}Fe_xO_3$ Single Crystals Grown by a Floating-Zone Method. *Phys. Rev. B* **2004**, *70* (6), 064426.

(29) Rado, G. T. Mechanism of Magnetoelectric Effect in an Antiferromagnet. *Phys. Rev. Lett.* **1961**, *6* (11), 609-.

(30) Abrahams, S. C.; Reddy, J. M.; Bernstein, J. L. Crystal Structure of Piezoelectric Ferromagnetic Gallium Iron Oxide. *J. Chem. Phys.* **1965**, *42* (11), 3957–3968.

(31) Bertaut, E. F.; Bassi, G.; Buisson, G.; Chappert, J.; Delapalme, A.; Pauthenet, R.; Rebouillet, H. P.; Aleonard, R. Etude Par Effet Mössbauer, Rayons X, Diffraction Neutronique et Mesures Magnétiques de $Fe_{1.15}Ga_{0.85}O_3$. *J. Phys.* **1966**, *27*, 433.

(32) Lefevre, C.; Roulland, F.; Thomasson, A.; Meny, C.; Porcher, F.; Andre, G.; Viart, N. Magnetic and Polar Properties' Optimization in the Magnetoelectric $Ga_{2-x}Fe_xO_3$ Compounds. *J. Phys. Chem. C* **2013**, *117* (28), 14832–14839. https://doi.org/10.1021/jp403733b.

(33) Stoeffler, D. First Principles Study of the Electric Polarization and of Its Switching in the Multiferroic $GaFeO_3$ System. *J. Phys.-Condens. Matter* **2012**, *24* (18), 185502.

(34) Kundys, B.; Roulland, F.; Lefevre, C.; Meny, C.; Thomasson, A.; Viart, N. Room Temperature Polarization in the Ferrimagnetic $Ga_{2-x}Fe_xO_3$ Ceramics. *J. Eur. Ceram. Soc.* **2015**, *35* (8), 2277–2281.

(35) Remeika, J. P. $GaFeO_3$: A Ferromagnetic-Piezoelectric Compound. *J. Appl. Phys.* **1960**, *31* (5), 263S.

(36) Roulland, F.; Lefevre, C.; Thomasson, A.; Viart, N. Study of $Ga(2-x)Fe_xO_3$ Solid Solution: Optimisation of the Ceramic Processing. *J. Eur. Ceram. Soc.* **2013**, *33* (5), 1029–1035. https://doi.org/10.1016/j.jeurceramsoc.2012.11.014.

(37) Trassin, M.; Viart, N.; Versini, G.; Barre, S.; Pourroy, G.; Lee, J.; Jo, W.; Dumesnil, K.; Dufour, C.; Robert, S. Room Temperature Ferrimagnetic Thin Films of the Magnetoelectric $Ga_{2-x}Fe_xO_3$. *J. Mater. Chem.* **2009**, *19* (46), 8876–8880. https://doi.org/10.1039/b913359c.

(38) Song, S.; Jang, H. M.; Lee, N.-S.; Son, J. Y.; Gupta, R.; Garg, A.; Ratanapreechachai, J.; Scott, J. F. Ferroelectric Polarization Switching with a Remarkably High Activation Energy in Orthorhombic $GaFeO_3$ Thin Films. *NPG Asia Mater* **2016**, *8*, e242. https://doi.org/10.1038/am.2016.3.

(39) Thomasson, A.; Cherifi, S.; Lefevre, C.; Roulland, F.; Gautier, B.; Albertini, D.; Meny, C.; Viart, N. Room Temperature Multiferroicity in $Ga_{0.6}Fe_{1.4}O_3$:Mg Thin Films. *J. Appl. Phys.* **2013**, *113* (21), 214101. https://doi.org/10.1063/1.4808349.

(40) Homkar, S.; Preziosi, D.; Devaux, X.; Bouillet, C.; Nordlander, J.; Trassin, M.; Roulland, F.; Lefèvre, C.; Versini, G.; Barre, S.; Leuvrey, C.; Lenertz, M.; Fiebig, M.; Pourroy, G.; Viart, N. Ultrathin Regime Growth of Atomically Flat Multiferroic Gallium Ferrite Films with Perpendicular Magnetic Anisotropy. *Phys. Rev. Mater.* **2019**, *3* (12), 124416. https://doi.org/10.1103/PhysRevMaterials.3.124416.

(41) Rojas-Sánchez, J.-C.; Reyren, N.; Laczkowski, P.; Savero, W.; Attané, J.-P.; Deranlot, C.; Jamet, M.; George, J.-M.; Vila, L.; Jaffrès, H. Spin Pumping and Inverse Spin Hall Effect in Platinum: The Essential Role of Spin-Memory Loss at Metallic Interfaces. *Phys. Rev. Lett.* **2014**, *112* (10), 106602.

(42)   Nguyen, M.-H.; Ralph, D. C.; Buhrman, R. A. Spin Torque Study of the Spin Hall Conductivity and Spin Diffusion Length in Platinum Thin Films with Varying Resistivity. *Phys. Rev. Lett.* **2016**, *116* (12), 126601. https://doi.org/10.1103/PhysRevLett.116.126601.

(43)   Nagaosa, N.; Sinova, J.; Onoda, S.; MacDonald, A. H.; Ong, N. P. Anomalous Hall Effect. *Rev. Mod. Phys.* **2010**, *82* (2), 1539–1592. https://doi.org/10.1103/RevModPhys.82.1539.

(44)   Hoffmann, A. Spin Hall Effects in Metals. *IEEE Trans. Magn.* **2013**, *49* (10), 5172–5193. https://doi.org/10.1109/TMAG.2013.2262947.

(45)   Sinova, J.; Valenzuela, S. O.; Wunderlich, J.; Back, C. H.; Jungwirth, T. Spin Hall Effects. *Rev. Mod. Phys.* **2015**, *87* (4), 1213–1259. https://doi.org/10.1103/RevModPhys.87.1213.

(46)   Zeissler, K.; Finizio, S.; Shahbazi, K.; Massey, J.; Ma'Mari, F. A.; Bracher, D. M.; Kleibert, A.; Rosamond, M. C.; Linfield, E. H.; Moore, T. A.; Raabe, J.; Burnell, G.; Marrows, C. H. Discrete Hall Resistivity Contribution from Néel Skyrmions in Multilayer Nanodiscs. *Nat. Nanotechnol.* **2018**, *13* (12), 1161–1166. https://doi.org/10.1038/s41565-018-0268-y.

(47)   Avci, C. O.; Garello, K.; Ghosh, A.; Gabureac, M.; Alvarado, S. F.; Gambardella, P. Unidirectional Spin Hall Magnetoresistance in Ferromagnet/Normal Metal Bilayers. *Nat. Phys.* **2015**, *11* (7), 570–575. https://doi.org/10.1038/nphys3356.

(48)   Guillet, T.; Zucchetti, C.; Barbedienne, Q.; Marty, A.; Isella, G.; Cagnon, L.; Vergnaud, C.; Jaffrès, H.; Reyren, N.; George, J.-M.; Fert, A.; Jamet, M. Observation of Large Unidirectional Rashba Magnetoresistance in Ge(111). *Phys. Rev. Lett.* **2020**, *124* (2), 027201. https://doi.org/10.1103/PhysRevLett.124.027201.

(49)   Lin, T. Magnetic Insulator Thin Films and Induced Magneto-Transport Effect at Normal Metal / Magnetic Insulator Interface, UC Riverside, 2013. https://escholarship.org/uc/item/8r22h4rt.

(50)   Guillemard, C.; Petit-Watelot, S.; Andrieu, S.; Rojas-Sánchez, J.-C. Charge-Spin Current Conversion in High Quality Epitaxial Fe/Pt Systems: Isotropic Spin Hall Angle along Different in-Plane Crystalline Directions. *Appl. Phys. Lett.* **2018**, *113* (26), 262404. https://doi.org/10.1063/1.5079236.

(51)   Sagasta, E.; Omori, Y.; Isasa, M.; Gradhand, M.; Hueso, L. E.; Niimi, Y.; Otani, Y.; Casanova, F. Tuning the Spin Hall Effect of Pt from the Moderately Dirty to the Superclean Regime. *Phys. Rev. B* **2016**, *94* (6), 060412. https://doi.org/10.1103/PhysRevB.94.060412.

(52)   Vila, L.; Kimura, T.; Otani, Y. Evolution of the Spin Hall Effect in Pt Nanowires: Size and Temperature Effects. *Phys. Rev. Lett.* **2007**, *99* (22), 226604. https://doi.org/10.1103/PhysRevLett.99.226604.

(53)   Zhou, X.; Ma, L.; Shi, Z.; Guo, G. Y.; Hu, J.; Wu, R. Q.; Zhou, S. M. Tuning Magnetotransport in PdPt/Y3Fe5O12: Effects of Magnetic Proximity and Spin-Orbit Coupling. *Appl. Phys. Lett.* **2014**, *105* (1), 012408. https://doi.org/10.1063/1.4890239.

(54)   Min, K.-J.; Chae, D.-H.; Kim, D.; Jeon, J.; Kim, T.; Joo, S. Electrically Controlled Magnetoresistance in Ion-Gated Platinum Thin Films. *J. Korean Phys. Soc.* **2019**, *75* (5), 398–403. https://doi.org/10.3938/jkps.75.398.

(55)   Ashcroft, N.; Mermin, N. *Solid State Physics*, New édition.; Brooks/Cole: New York, 1976.

(56)   Anadón, A.; Guerrero, R.; Jover-Galtier, J. A.; Gudín, A.; Díez Toledano, J. M.; Olleros-Rodríguez, P.; Miranda, R.; Camarero, J.; Perna, P. Spin-Orbit Torque from the Introduction of Cu Interlayers in Pt/Cu/Co/Pt Nanolayered Structures for Spintronic Devices. *ACS Appl. Nano Mater.* **2021**, *4* (1), 487–492. https://doi.org/10.1021/acsanm.0c02808.

(57)   Luan, Z. Z.; Chang, F. F.; Wang, P.; Zhou, L. F.; Cooper, J. F. K.; Kinane, C. J.; Langridge, S.; Cai, J. W.; Du, J.; Zhu, T.; Wu, D. Interfacial Coupling and Negative Spin Hall Magnetoresistance in Pt/NiO/YIG. *Appl. Phys. Lett.* **2018**, *113* (7), 072406. https://doi.org/10.1063/1.5041865.

(58)   Lin, T.; Tang, C.; Shi, J. Induced Magneto-Transport Properties at Palladium/Yttrium Iron Garnet Interface. *Appl. Phys. Lett.* **2013**, *103* (13), 132407. https://doi.org/10.1063/1.4822267.

(59) Lin, T.; Tang, C.; Alyahayaei, H. M.; Shi, J. Experimental Investigation of the Nature of the Magnetoresistance Effects in Pd-YIG Hybrid Structures. *Phys. Rev. Lett.* **2014**, *113* (3), 037203. https://doi.org/10.1103/PhysRevLett.113.037203.

(60) Ko, H.-W.; Park, H.-J.; Go, G.; Oh, J. H.; Kim, K.-W.; Lee, K.-J. Role of Orbital Hybridization in Anisotropic Magnetoresistance. *Phys. Rev. B* **2020**, *101* (18), 184413. https://doi.org/10.1103/PhysRevB.101.184413.

(61) Meunier, B.; Homkar, S.; Lefèvre, C.; Roulland, F.; Pourroy, G.; Salluzzo, M.; Preziosi, D.; Viart, Nathalie. Spin Reorientation Transition in Multiferroic Gallium Thin Films Evidenced by Temperature Dependent X-Ray Magnetic Dichroism Experiments. *Manuscript under preparation*.